New Zealand Journal of Geology and Geophysics, 2013
http://dx.doi.org/10.1080/00288306.2013.802246

Taylor & Francis
Taylor & Francis Group

RESEARCH ARTICLE

The sub-Antarctic Antipodes Volcano: a <0.5 Ma HIMU-like Surtseyan volcanic outpost on the edge of the Campbell Plateau, New Zealand

JM Scott*, IM Turnbull, A Auer and JM Palin

Department of Geology, University of Otago, Dunedin, New Zealand

(*Received 10 February 2013; accepted 19 April 2013*)

The sub-Antarctic Antipodes Islands group, located on the edge of the Campbell Plateau, is composed of Surtseyan-like tuff cones, porphyritic lavas and dykes, overlain by scoriaceous cinder cones. The youthful nature is indicated by well-preserved cones and craters, raised boulder beaches, pollen and spores comparable to the present-day vegetation in peat underlying one lava flow, and published Ar/Ar ages of ≤ 0.5 Ma. The alkaline crystalline rocks record a fractionation lineage that was controlled by progressive removal of clinopyroxene and olivine at shallow depths with minimal interaction with continental crust. A compilation of isotopic data confirms that the magmas were derived from a mantle source containing a high-time integrated U/Pb (HIMU)-like component. Although this source component has been recognised in many Zealandia intraplate volcanoes, the Antipodes Volcano lavas contain consistently high $^{206}Pb/^{204}Pb$ and low $^{87}Sr/^{86}Sr$ ratios, making the geochemical suite an excellent baseline for HIMU studies. The distinctive isotope ratios and chemistries are comparable with those of some anhydrous Pb- and K-depleted peridotitic mantle xenoliths from intraplate volcanoes in Zealandia. If the lithospheric mantle contributed to the source of Antipodes Volcano, the Pb and K anomalies in the lavas may not require residual amphibole/phlogopite and/or sulphide in their source region. Furthermore, comparison with the peridotite suite indicates that the Zealandia lithospheric mantle is isotopically heterogeneous and thus not all the Zealandia Cretaceous–Cenozoic intraplate volcanoes need have tapped a HIMU-like reservoir.

Keywords: alkaline volcanism; Antipodes Islands; geochemistry; geological map; HIMU

Introduction

Small-volume alkaline intraplate magmas with high time-integrated U–Pb signatures (HIMU) have repeatedly punctured New Zealand's continental crust (Zealandia) over the last c. 95 Ma. The petrology of these volcanoes, which share chemical similarities with volcanoes in Antarctica (Panter et al. 2000) and southeast Australia (Lanyon et al. 1993; Zhang et al. 1999) but not the intervening ocean basins, has been subject to extensive investigation during the last three decades (e.g. Coombs et al. 1986, 2008; Gamble et al. 1986; Barreiro & Cooper 1987; Weaver & Smith 1989; Baker et al. 1994; Price et al. 2003; Finn et al. 2005; Hoernle et al. 2006; Panter et al. 2006; Sprung et al. 2007; Timm et al. 2009, 2010; McCoy-West et al. 2010; Mortimer et al. 2012). This 'diffuse alkaline magmatic province' (DAMP; Finn et al. 2005) is geologically significant because the volcano chemistries record a complex two-stage process involving: (1) the regional formation of a HIMU-type reservoir; and (2) subsequent repeated tapping of this enriched source (along with mixing within other domains). The origin and cause of both processes remain debated (Hoernle et al. 2006; Panter et al. 2006; Sprung et al. 2007).

Although the best-studied intraplate volcanic provinces occur on the New Zealand mainland (e.g. Alpine Dike Swarm (Barreiro & Cooper 1987); Dunedin Volcanic Group (Price et al. 2003; Hoernle et al. 2006; Coombs et al. 2008); Lyttelton and Akaroa volcanoes (Timm et al. 2009); Lookout Volcanics (McCoy-West et al. 2010); and Tapuaenuku Igneous Complex (Baker et al. 1994)), $>90\%$ of Zealandia is currently submerged. Some insights into the offshore intraplate magmatism have been gained through dredge samples (Timm et al. 2010; Mortimer et al. 2012), collection material from volcanoes on the Chatham Islands (Morris 1985a,b; Panter et al. 2006; Sprung et al. 2007) and examination of existing but sparse geological collections from uninhabited sub-Antarctic Islands (Gamble et al. 1986; Hoernle et al. 2006; Panter et al. 2006; Timm et al. 2010). Due to the difficulty in accessing the sub-Antarctic Islands, comparatively little is known about most of these offshore volcanic centres.

We build upon the existing small, albeit high-quality, published geochemical and isotopic dataset from the sub-Antarctic Antipodes Islands (49°40'S, 178°45'E) by providing the first detailed geological map and lithological description of units and interpreting the petrological history and source region of the Antipodes Volcano. This tiny volcanic outpost, 800 km southeast of the New Zealand mainland, erupted through the continental Campbell Plateau very close to the edge of Zealandia continental crust (Fig. 1). Published data show that Antipodes Volcano lavas have some of the highest

*Corresponding author. Email: james.scott@otago.ac.nz
Supplementary data available online at www.tandfonline.com/10.1080/00288306.2013.802246
Supplementary file: Figure S1. Trace-element-normalised concentrations for individual whole rock analyses.

$^{206}Pb/^{204}Pb$ values of all the DAMP volcanic rocks across Zealandia (Panter et al. 2006; Timm et al. 2010). However, the field context of the previously analysed lavas has not been presented, and the petrology of the volcanic complex as a whole is unknown. Previous field and petrographical information on the Antipodes Islands is restricted to reconnaissance descriptions made by Hector (1870), Cullen (1969) and Adams (1985), who presented petrological and/or K–Ar data from the northeast coast. Gamble et al. (1986) interpreted existing Antipodes Volcano petrological data in a regional context. The new field and geochemical data enable us to provide a synthesis of the magmatic petrology of the Antipodes Volcano and, compared with new isotopic data, place the high-μ (HIMU) -like mantle signal in both local and regional context.

Geology

The Antipodes Islands sit upon a roughly 35 km × 15 km pedestal that is elongated towards the northeast (Cullen 1969). The sea floor drops away rapidly to the Sub-Antarctic Slope just 10 km southeast of the islands. The island group is composed of the central Antipodes Island (6 km × 6 km at its longest dimensions), the small (c. 1 km × 1 km) Bollons Island to the north and several tiny islets (Fig. 2). Exposure away from the coasts is poor, being commonly obscured by up to 5 m of peat and thick tussock and fern cover. We estimate Antipodes Island to be composed of about 80% bedded pyroclastic material, 15% lava and 5% scoria. Bollons Island rises to about 200 m and has a profile reminiscent of an eroded c. 1 km wide volcanic crater. It is composed entirely of bedded pyroclastic material. Photographic reconnaissance and a circumnavigation of the island group by boat indicate that the extremely steep-sided Leeward Islet and the Windward Islets are also composed entirely of bedded pyroclastic material. South Islet is probably composed of lava.

The youthful volcanic nature of the Antipodes Islands group, first noted by Hector (1870), was confirmed by

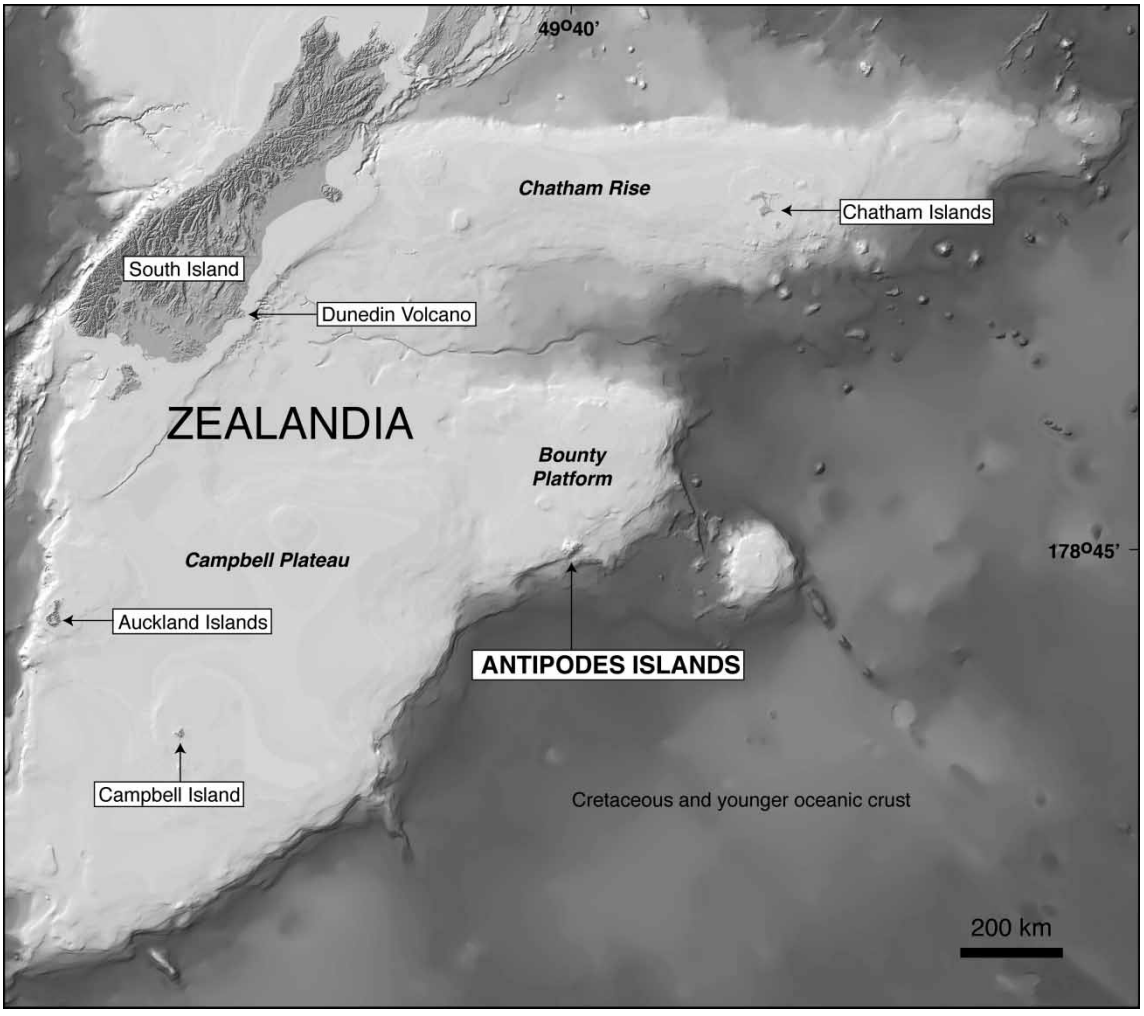

Figure 1 Bathymetric map of Zealandia illustrating the location of the Antipodes Islands on the edge of the Bounty Platform section of the Campbell Plateau. Image modified from bathymetric map obtainable free from the National Institute of Water and Atmospheric Research.

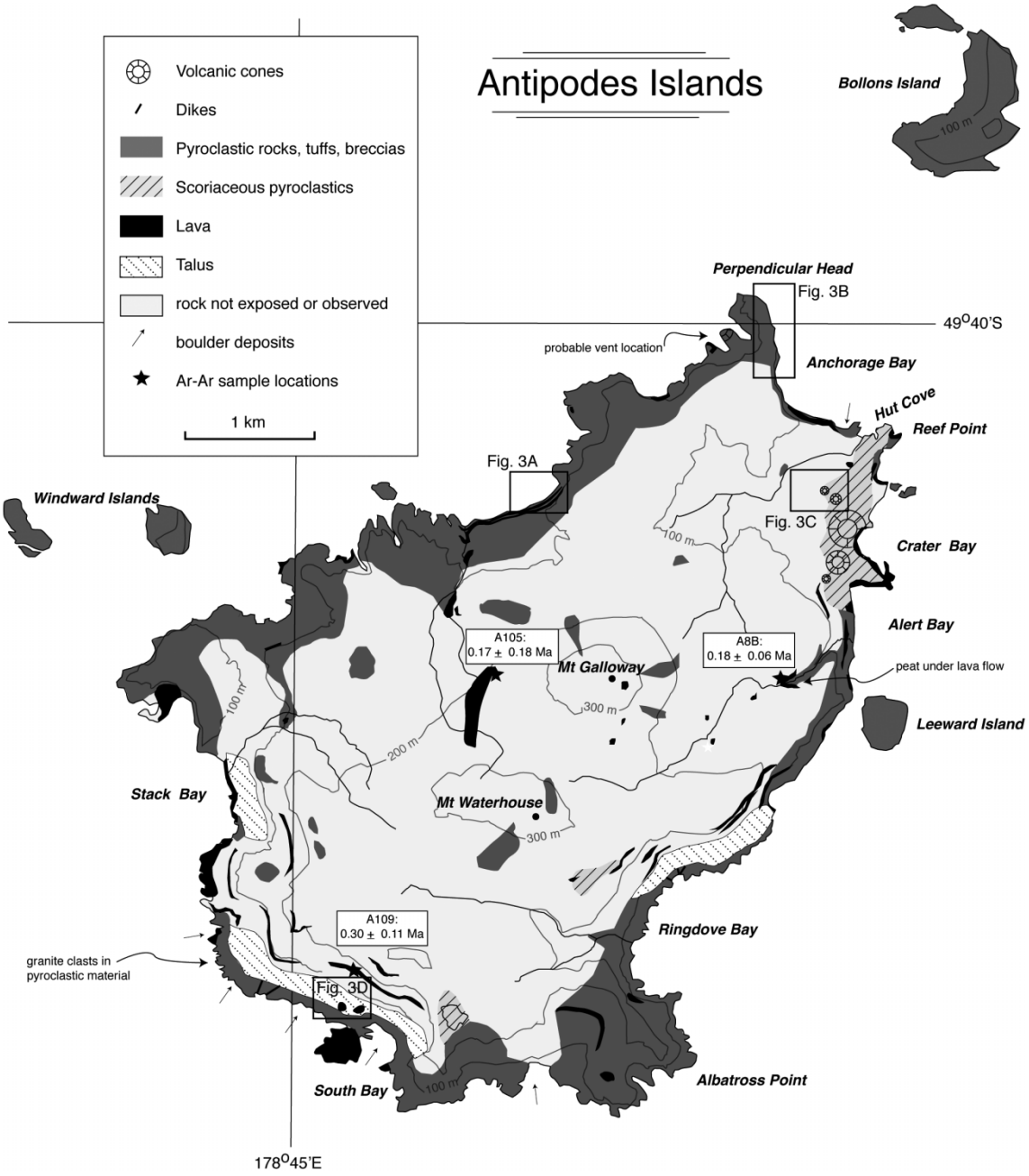

Figure 2 Geological map of the Antipodes Islands showing geographic features and $^{40}Ar/^{39}Ar$ age data locations (ages from Timm et al. 2010).

imprecise K–Ar Pleistocene dates (Cullen 1969; Adams 1985) and, more recently, by Timm et al. (2010) who found that several specimens collected by Reay et al. (1990) have eruption (Ar/Ar) ages of <0.5 Ma.

Lavas

Lava flows are widely but sparsely distributed across the main island (Fig. 2). Many of these flows are distinctive because they exhibit prominent columnar jointing. Pillow lavas were not found. The flows commonly have a fine-grained base and a rubbly top, are mostly subhorizontal and in places reach c. 20 m in thickness. Some of the flows above South Bay tend to dip northwards (Reay et al. 1990). There are multiple extrusions, as illustrated in successive layering of flows within the cliffs above Ringdove Bay, South Bay and opposite Orde Lees Islet (Fig. 3A). Alert Bay exposes a stack of 2–3 m thick lavas separated by coarse ash-lapilli tuff and agglomerate horizons. Immediately south of Stack Bay, an extensive lava flow has a columnar-jointed top that grades into a central portion that has a strong platy flow fabric. Elongate vesicles define more subtle flow fabrics

elsewhere on the island, but no systematic orientation has been established.

There is no obvious vertical stratigraphy to the lavas, but there are geographical differences in composition. Porphyritic varieties are commonly found in, although not restricted to, the northern portion of the island. Porphyritic lavas commonly contain large (up to 1 cm) subhedral crystals of clinopyroxene + olivine and/or rare plagioclase set among a fine-grained matrix consisting of plagioclase laths, microphenocrysts of clinopyroxene and olivine, apatite and densely packed opaque minerals of varying grainsize (Fig. 4A). The base of the lavas commonly contains a larger content of phenocrysts relative to the top of the lava. Olivine phenocrysts do not appear to be appreciably zoned on the basis of petrographic observations. However, coarse clinopyroxene grains commonly have a thin slightly darker and embayed rim compared to the core. Plagioclase phenocrysts are also zoned; they commonly exhibit a growth hiatus marked by fine opaque minerals and a sieve-textured core. Kaersutite is present in some porphyritic lavas. Fine-grained pale grey lavas occur on the southern side of Antipodes Island. These lavas contain euhedral plagioclase phenocrysts up to 1 mm long set within a trachytic matrix of needles of fine-grained feldspar. The large feldspar phenocrysts tend to be inclusion-free (Fig. 4B).

Dykes

Dykes are uncommon; the few observed are on the southern coast, in Ringdove Bay opposite Orde Lees Islet (Cullen 1969), and on the western side of Perpendicular Point. At the latter location a dyke several metres thick exposed in a cliff face has intruded through pyroclastic rocks, branched into a sill and then fed a subhorizontal lava flow. Dykes are generally 03–1.5 m wide, with a moderate to subvertical dip. The strike orientations of dykes are not consistent along the length of an individual dyke, and there are no systematic orientations. Platy margins and elongate flow-oriented vesicles are common. Dyke rocks are porphyritic with subequal proportions of olivine and clinopyroxene phenocrysts set in a fine-grained matrix of feldspar and opaque minerals.

Pyroclastic rocks

Although lavas are prominent features, the bulk of Antipodes Island is composed of bedded pyroclastic rocks. These form continuous piles that are up to 150 m thick with few or no intervening lavas (Fig. 3B). Pyroclastic beds clearly drape the edges of lava flows on Perpendicular Head and Albatross Point. The southern end of Ringdove Bay exposes red-weathering pyroclastic material that is overlain by a columnar

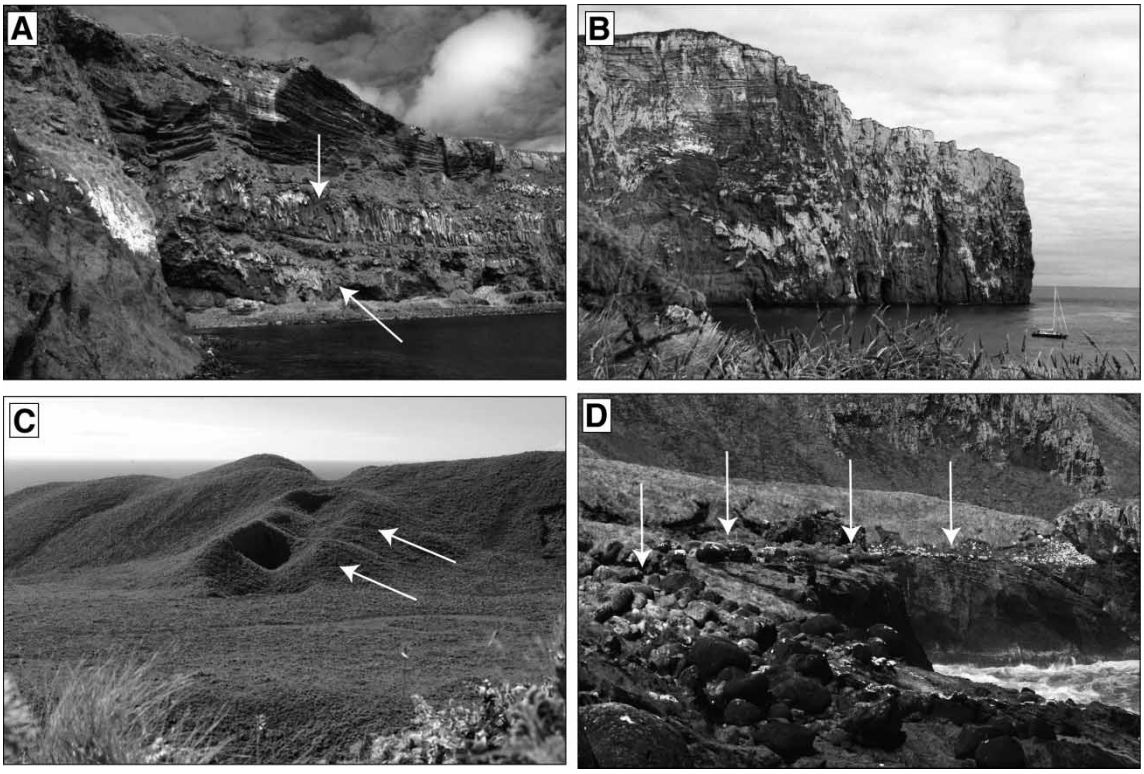

Figure 3 Field images from the Antipodes Island (the locations of photos are shown in Fig. 2). **A**, Two columnar-jointed lava flows (arrowed), separated by an oxidised horizon and overlain by bedded pyroclastic deposits, occur in the cliff face on the northwest side of the main Antipodes Island. **B**, c. 180 m of bedded pyroclastic deposits make up Perpendicular Head. Note the 15-m-long yacht for scale. **C**, Small cinder cones occur on the northeast corner of the island. **D**, Large rounded boulders sitting upon an erosion surface, about 10 m above current sea level, at South Bay.

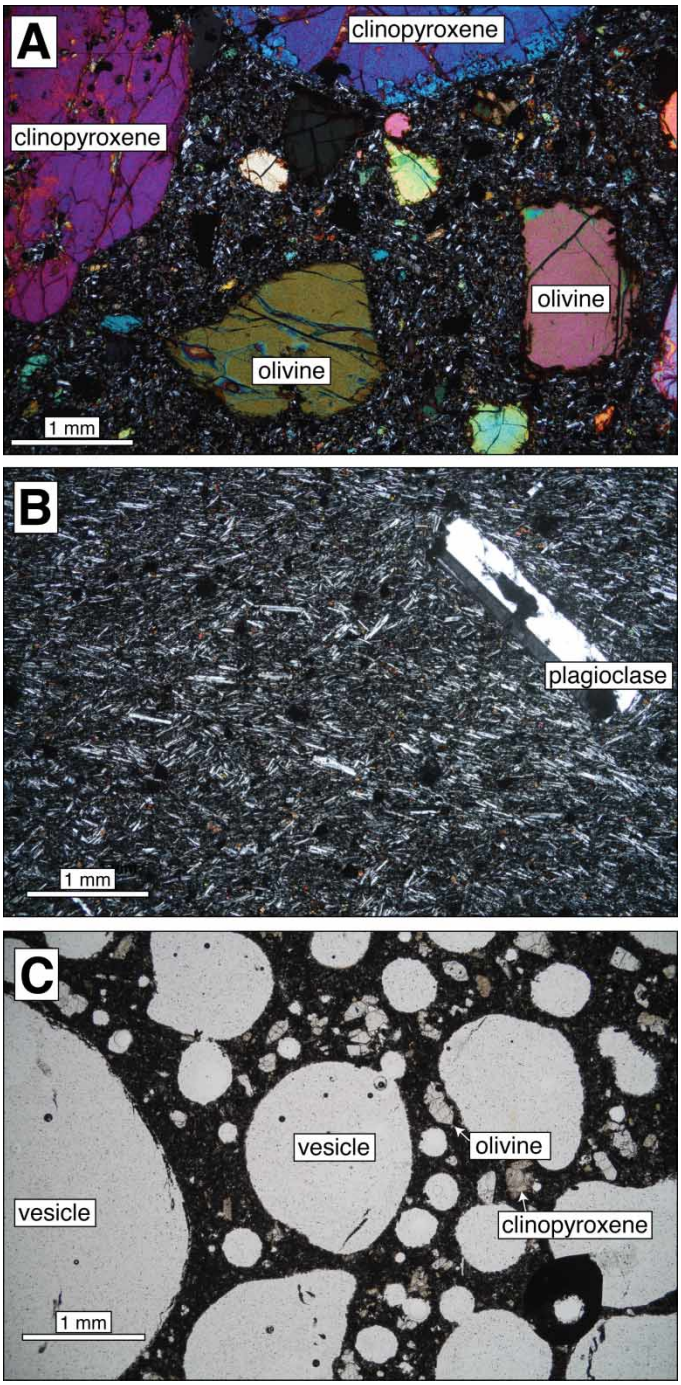

Figure 4 Microscopic views of Antipodes lavas. **A**, Porphyritic basanite with large clinopyroxene and olivine phenocrysts; **B**, large plagioclase phenocryst within a trachytic groundmass; **C**, an example of vesicular scoria.

jointed flow, both of which have in turn been truncated by a steep cliff and then overlain by a thick succession of pyroclastic beds that also drape the cliff. The pyroclastic beds also contain numerous angular unconformities, with bedding regularly truncated and then overlain by pyroclastic horizons dipping in a different direction. On the southern coastal cliffs southwest of Albatross Point about 10 m above sea level, pyroclastic rocks with thin inter-bedded flows dipping east at c. 50° and cut by dykes have been truncated by an erosion surface, overlain by a boulder beach deposit and then buried by at least 100 m of flat-lying pyroclastic sediments (the whole intruded by a younger dyke; Fig. 5).

Bedded pyroclastic rocks are layered on a centimetre–decimetre scale. However, the bedding orientations commonly vary widely and no pattern is recognised. As ripple marks were not seen and cross bedding is rare, most of the pyroclastic

rocks observed appear to have been sub-aerially deposited. The pyroclastic deposits strongly resemble classic Surtseyan tuff cones described by Lorenz (1974) and Verwoerd & Chevallier (1987), which means the variable bedding orientations may represent the outlines of eruption centres. Apparent 'faults' in the pyroclastic sequences, such as on Perpendicular Head (as noted by Cullen 1969), may therefore be due to slumping of wet weakly consolidated tuff cone margin during the eruptive sequence.

The most widespread pyroclastic lithology observed is coarse tuff to lapilli-tuff. This facies is commonly poorly sorted and contains cognate blocks of fine-grained and porphyritic lava, as well as reworked blocks of ash or lapillistone. The largest clasts (up to 1 m) are almost invariably angular blocks of lava that had already crystallised before being entrained during eruptions. Poorly to unsorted coarse ash-lapilli breccia with blocks of angular lava and reworked pyroclastic material occur at sea level in Ringdove Bay, east of Albatross Point, on the shoreline west of South Bay and north of Orde Lees Islet. Clinopyroxene phenocrysts up to c. 1 cm diameter occur in ash-lapilli-tuff to the west of South Bay. Subordinate amounts of coarse vitric tuff and lithic-crystal tuff with euhedral fresh augite and rare olivine crystals are also present.

Scoria deposits

Loose and unweathered scoria deposits form about 5% of Antipodes Island. Many of the vent-shaped features inferred by Cullen (1969), Warham & Jones (1975) and Thomson (1990) could not be confirmed from field mapping due to the thick vegetative cover, but several small cinder cones clearly occur on the northeast corner of the island (Fig. 3C). These vents are composed of red-brown weathering and highly vesicular and partially welded scoria containing spindle bombs and clasts with bread-crust texture, as well as ropy agglutinated spatter. There is also a well-preserved crater above Alert Bay. Here, a pedestal of columnar jointed lava is overlain by a succession of c. 1–5 m layered, red-brown, vesicular and fine-grained lava and pyroclastic beds. Other highly vesicular scoriaceous deposits and lavas occur on the peninsula extending out from South Bay, on a peak southwest of Albatross Point, above Ringdove Bay, on the western side of Perpendicular Point and extending to the sea at Reef Point.

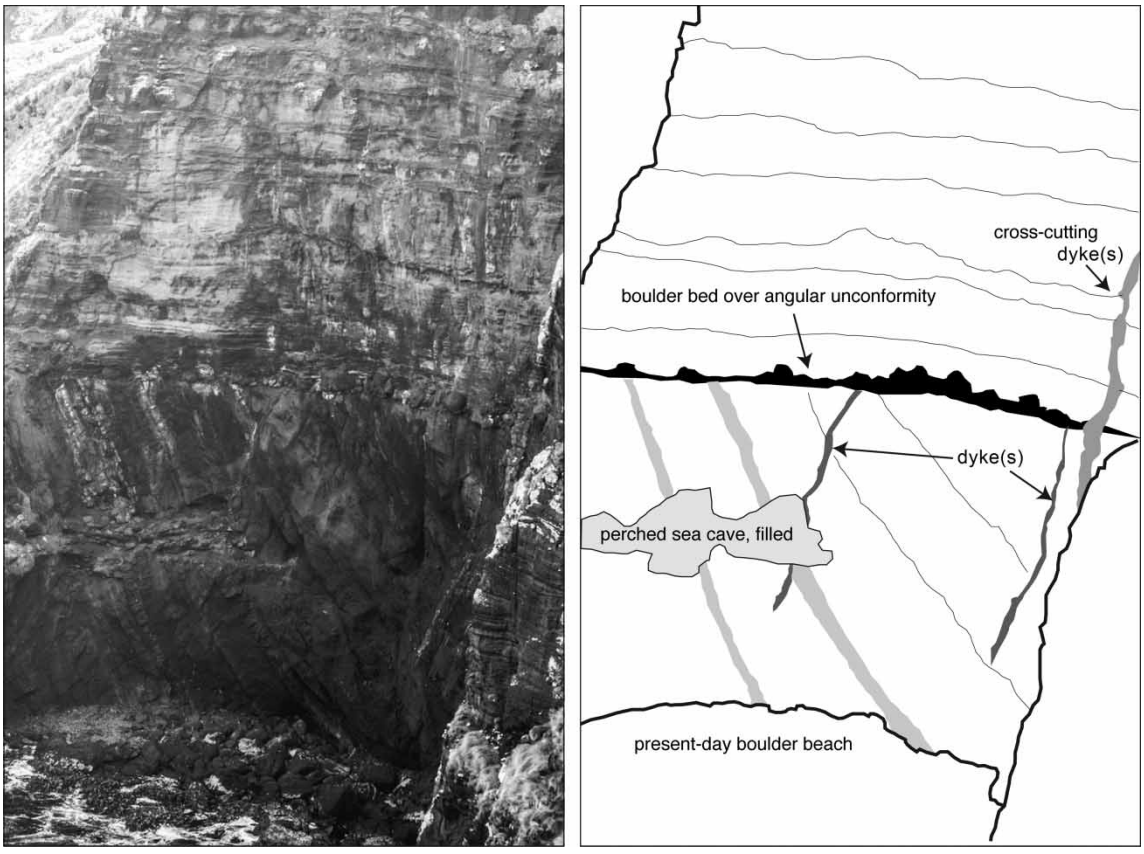

Figure 5 Photo (left) and sketch (right) of a cliff face west of Albatross Point, c. 50 m high. Pyroclastic sediments with probable interbedded flows dip c. 50° east, and are cut by two thin dykes. This lower dipping sequence has been truncated by a horizontal marine erosion surface littered with boulders, c. 20 m above current sea level. This boulder beach is overlain by horizontally bedded pyroclastic rocks that extend to the top of Reliance Ridge, 200 m above. A younger dyke cuts the entire sequence. A perched (possibly submarine) sea cave in-filled with boulders is preserved below the main boulder bed.

The scoriaceous material is highly vesicular and contains subhedral microphenocrysts of clinopyroxene and olivine in a fine-grained and commonly altered matrix (Fig. 4C).

Exotic rocks

Exotic rocks in the volcanic pile are rare. Adams (1985) reported a single coarse-grained gabbro xenolith from a basalt beach boulder. The only other obviously exotic inclusions which have been discovered are extremely rare granitic xenoliths found within pyroclastic rocks west of South Bay; single small xenoliths were noted at Ringdove Bay and Hut Cove. The xenoliths are angular to subrounded and typically range between 1 and 4 cm in diameter, although a 10 cm diameter specimen was previously collected from west of South Bay (Reay et al. 1990) and has a Mesozoic zircon U–Pb age (Tulloch et al. 2003). Although most xenoliths are enclosed directly within the ash-lapilli tuff, several were found enclosed within fine-grained basaltic blocks that have been reworked into the tuff. The granitic xenoliths are heavily corroded and melted, with primary feldspar having been destroyed. They are now composed of quartz, variably altered pale glass, an opaque phase and fine-grained zircon.

Boulder beach deposits

Distinctive boulder horizons up to several metres thick occur at numerous places around the island. These horizons are particularly prominent in the cliffs east of Orde Lees Islet, near Alert Bay, and along the southern coast (Figs 3C, 5). Most are bouldery with clasts from 25 cm to 1 m in diameter to a maximum of c. 5 m, although beach gravels with pebbles around 2–3 cm do occur (e.g. in central Ringdove Bay; cf. Adams 1985). The boulders are locally derived lavas, never of pyroclastic material. All clasts are well rounded and many are spherical. The matrix of these deposits is reworked pyroclastic material, commonly cemented, but non-calcareous. Boulder deposits are at various heights above current sea level, mostly c. 10 m, but occasionally deposits are preserved up to 20 m or as low as 2–5 m above the high tide mark. Some can be seen filling elevated (stranded) sea caves, whereas others are clearly within the pyroclastic–lava sequence (see Fig. 5). No fossils have yet been found in any of these deposits.

Surficial deposits

Fine-grained peat up to 5 m thick blankets all but the steepest slopes of Antipodes Island, and peaty soil covers the western slopes of Bollons Island and flatter slopes on the other offshore stacks. The peat is prone to landslides when saturated and scarps or scars provide the only exposures of underlying pyroclastic rocks. The peat is also prone to tunnel gullying, and collapsed underground stream cavities are the origin of numerous pits seen in aerial photographs (Thomson 1990). Slopes above Ringdove, South and Stack bays are mantled with slope wash and colluvium, this debris being derived from disintegration of previously steeper cliffs. These slopes are currently cliffed at the base, and have the same origin as the two-storied cliffs described from the Auckland Islands by Fleming (1965).

At a waterfall in Dougall Stream, pyroclastic rocks are overlain by carbonaceous mudstone and baked peat (lignite) in a sequence c. 3 m thick. The peat contains fern spores and grass pollen typical of the present-day vegetation on the island (J.I. Raine, pers. comm. 2012). The pollen suite also contains podocarp spores, which may be due to long-distance wind transport since there is no firm evidence of trees having been present on the island at any time, although a possible charcoal log was found in pyroclastic sediments at Ringdove Bay. *Nothofagus* and podocarp pollen has been transported from the New Zealand mainland as far south as Campbell Island (McGlone & Muerk 2000).

Whole-rock geochemistry

Twenty fresh crystalline rocks from across the main Antipodes Island were processed for whole-rock major and trace-element geochemistry (Fig. 6A). Major elements were measured by X-ray fluorescence on lithium metaborate fused glass disks and trace elements measured by inductively coupled plasma mass spectrometry (ICP-MS) following four-acid (perchloric, hydrofluoric, nitric and hydrochloric) digestion (both at ALS Ltd, Australia). Loss on ignition was conducted by furnace heating of a powder fraction. Iron was measured and reported in Table 1A–C as Fe_2O_3 but mathematically converted to $FeO_{(total)}$ for the purpose of calculating Mg#. This dataset is supplemented by data for three lavas presented by Panter et al. (2006) (Ant 7, Ant 13, Ant 16) and ten lavas analysed by Timm et al. (2010) (A2, A5, A6, A8b, A23a, A102, A105, A109, A108, A112) but collected by Reay et al. (1990). Four analyses from Anchorage Bay and Reef Point presented by Gamble & Adams (1990) and data from Cullen (1969) are not included because there are already three analyses from the same lava flows in our own collection and two from the Panter et al. (2006) dataset.

New and published whole-rock geochemical analyses are listed in Table 1A–C. A total alkali versus SiO_2 diagram for all data shows that the lava compositions range from picrobasalt and basanite (normative olivine $> 10\%$) through to trachyandesite or tephra-phonolite (Fig. 6B). On the basis of $Na_2O - K_2O > 2$, the trachyandesite can be further classified as benmoreite and the basaltic trachyandesite classified as mugearite (Gill 2010). All the samples are nepheline-normative and hence strongly silica undersaturated. Fenner diagrams illustrate smooth overall trends in major (Fig. 7) and minor elements (Fig. 8). Rocks with the highest MgO have the lowest Al_2O_3, K_2O, Na_2O, P_2O_5 and SiO_2 contents (Fig. 7). TiO_2 and FeO contents initially increase with decreasing MgO but begin to

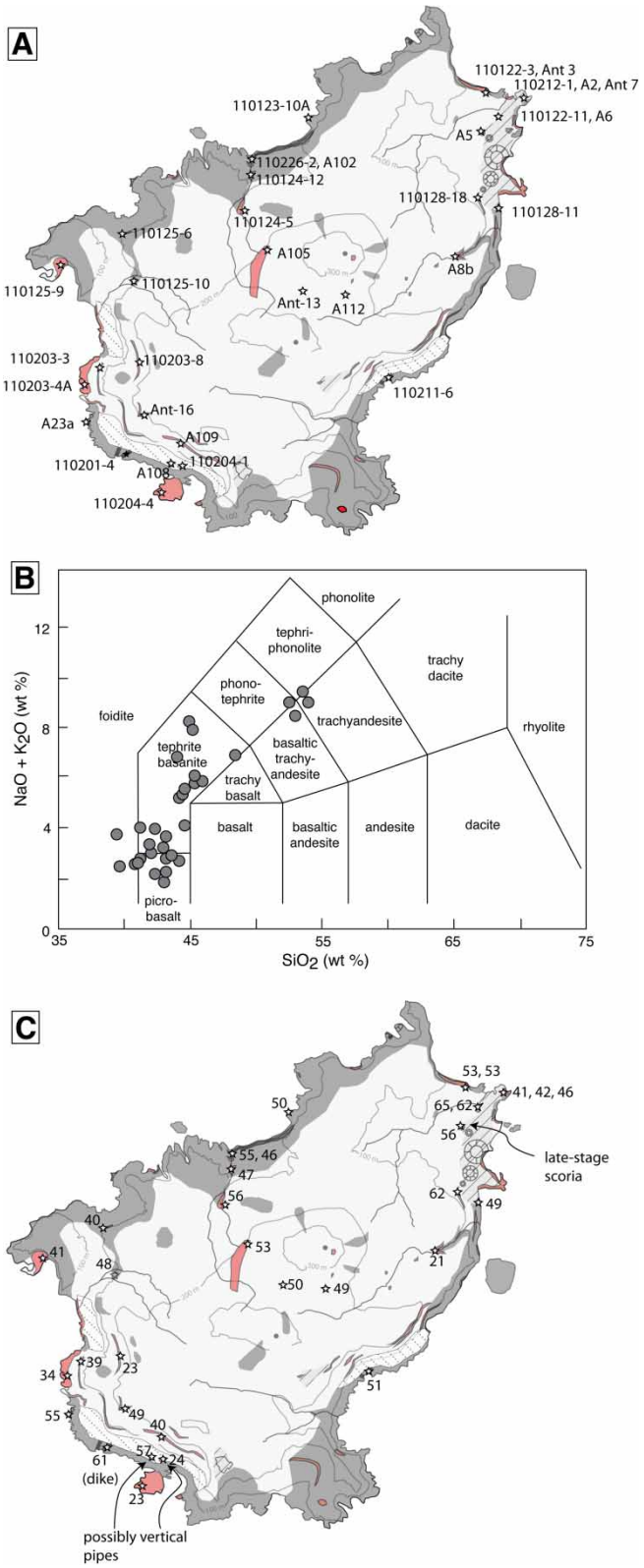

Figure 6 Geochemical properties of lavas. **A**, Locations of geochemically sampled lavas (prefix 110), including data presented in Panter et al. (2006) (sample prefix Ant) and Timm et al. (2010) (sample prefix A). **B**, Total alkalis versus silica classification diagram for geochemical samples. Diagram from Le Maitre et al. 2002. **C**, Magnesium numbers (= mol. $Mg/(Mg + Fe^{total}) \times 100$) for all samples.

Table 1A New and published whole-rock geochemical data for the Antipodes Volcano, sorted by Mg#.

	110122–11	110128–18	A6	110201–4	A108	A5	110124–5	A23a	110126–2	Ant 3	A105
	Scott et al.	Scott et al.	Timm et al.	Scott et al.	Timm et al.	Timm et al.	Scott et al.	Timm et al.	Scott et al.	Panter et al.	Timm et al.
Lat.,	49°40.167	49°40.690		49°42.360			49°40.831		49°40.443		
Long	178°48.377	178°48.381		178°44.576			178°45.910		178°45.896		
SiO_2	43.00	43.50	42.34	44.20	43.19	39.41	41.10	43.09	41.20	43.17	40.75
TiO_2	2.91	3.03	3.29	2.75	3.67	3.75	4.01	3.77	4.05	4.11	4.24
Al_2O_3	8.38	10.30	9.55	10.45	10.90	11.42	10.10	12.08	10.40	11.48	10.66
Fe_2O_3	15.55	14.95	1.68	15.50	1.64	1.64	17.35	1.65	17.50		1.82
FeO			14.93		14.57	14.61		14.72		15.67	16.19
MnO	0.18	0.18	0.18	0.20	0.16	0.18	0.20	0.17	0.20	0.20	0.18
MgO	14.80	12.50	13.72	12.40	10.73	10.56	11.15	10.17	10.85	9.88	10.42
CaO	12.95	12.10	11.65	10.75	11.97	11.43	12.85	11.55	12.55	11.88	12.74
Na_2O	1.48	2.16	1.67	2.13	1.74	2.76	1.98	2.12	2.09	2.33	1.94
BaO	0.02	0.03		0.02			0.03		0.02		
K_2O	0.42	0.78	0.50	0.60	0.55	0.99	0.66	0.66	0.69	0.52	0.68
P_2O_5	0.31	0.50	0.41	0.40	0.37	0.96	0.58	0.43	0.64	0.76	0.64
Cr_2O_3	0.11	0.08		0.07			0.06		0.05		
SrO	0.04	0.06		0.05			0.07		0.07		
LOI	−0.30	−0.32	0.65	0.19	0.74	1.71	−0.40	0.59	−0.43	−0.18	0.56
	99.85	**99.85**	**100.57**	**99.71**	**100.23**	**99.42**	**99.74**	**101.00**	**99.88**	**99.82**	**100.82**
Ba	110	190	141	150	143	334	170	171	180	250	190
Cr	505	375	532	323	318	291	247	323	230	365	379
Cu	46.9	80.4	32.9	113.5	29.9	61.8	36.2	29.9	44.2	44	27.7
Ga	16.55	19.55	18.1	19.4	20.2	23.4	21.4	22.1	21.6	22	22.6
La	21.3	32.2	23.5	26	18.9	50.8	34.4	25.2	36	31.1	31.6
Nb	23.8	40.8	29.7	30.3	26.7	65.1	38.5	33.2	39.6	44	37.4
Ni	258	256	268	269	155	239	149	159	147	148	162
Pb	0.6	1.9	0.93	2.6	1.52	2.11	1.7	1.52	1.6	1.3	1.29
Rb	8.8	18.4	9.87	13.5	10.7	25.3	15.7	14.2	15.5	17	15.8
Sc	37.8	29.7	33.9	27.9	35.4	24	32.8	32	30.8	32.4	33.9
Sr	353	499	428	451	433	905	603	531	633	530	641
Th	2.2	3.7	2.38	3	2.14	5.12	3.3	2.61	3.4	2.9	2.77
U	0.6	0.9	0.66	0.8	0.61	1.33	0.9	0.42	0.9	0.9	0.74
V	301	273	340	257	411	280	377	417	368	351	468
Y	20	23.1	22.4	21.9	19.9	30.9	26.1	24.1	26.7	30	27.9
Zn	104	117	131	138	126	153	125	135	127	135	147
Zr	145.5	196	170	174.5	158	293	216	187	221	232	226
Dy	3.98	4.62	4.45	4.23	3.93	6.38	5.18	4.6	5.24		5.44
Er	1.82	2.07	1.83	1.98	1.62	2.34	2.36	1.92	2.41		2.2
Eu	1.87	2.27	2.06	2.02	1.82	3.47	2.62	2.1	2.69	4.64	2.66
Gd	5.27	6.35	5.73	5.6	4.93	9.32	7.37	5.81	7.5		7.34
Ho	0.71	0.83	0.77	0.78	0.68	1.03	0.92	0.79	0.94		0.92
Lu	0.17	0.19	0.19	0.2	0.16	0.21	0.22	0.19	0.22	0.25	0.21
Nd	23.2	30.9	28.3	25.8	23.3	55.8	35.7	29.1	37.2	72	38.7
Pr	5.43	7.52	6.76	6.2	5.56	13.9	8.53	7.04	8.83		9.26
Sm	5.46	6.75	6.28	5.81	5.33	11.2	7.79	6.39	7.98	15.6	8.25
Tb	0.8	0.94	0.85	0.85	0.75	1.32	1.08	0.87	1.09	1.62	1.07
Tm	0.21	0.24	0.23	0.24	0.2	0.28	0.27	0.25	0.28		0.27
Yb	1.21	1.35	1.4	1.38	1.22	1.59	1.57	1.46	1.56	2.25	1.62
Mg#	65	62	62	61	57	56	56	55	55	53	53
Nepheline	4.78	6.25	4.62	2.41	2.46	12.65	7.92	4.43	7.77	4.07	8.08
Diopside	38.74	33.41	30.96	27.61	30.01	28.32	35.82	27.06	34.10	28.34	33.41
Olivine	26.25	23.13	28.86	25.98	22.88	23.14	21.24	23	21.40	20.97	22.48

Table 1B New and published whole-rock geochemical data for the Antipodes Volcano, sorted by Mg#.

	110122–3A	110211–6	110123–10A	Ant 13	A112	Ant 16	110125-10	110124-12	Ant 7	A102	110128-11
	Scott et al	Scott et al	Scott et al	Panter et al.	Timm et al	Panter et al.	Scott et al.	Scott et al.	Panter et al.	Timm et al.	Scott et al.
Lat.,	49°40.039′	49°41.875′	49°40.184′				49°41.237	49°40.623			49°40.690
Long	178°48.376′	178°47.307′	178°46.463′				178°44.760	178°45.961			178°48.381
SiO_2	42.10	42.90	44.40	41.96	39.60	43.15	44.50	42.30	43.99	41.19	44.10
TiO_2	4.10	3.94	3.04	4.42	4.39	4.64	3.71	4.52	3.50	4.29	3.81
Al_2O_3	11.10	12.55	13.55	12.70	11.99	13.13	14.10	13.05	13.86	12.95	14.95
Fe_2O_3	17.40	16.50	14.85		1.86		15.55	17.10		1.78	14.95
FeO				15.92	16.55	15.46			13.60	15.85	
MnO	0.20	0.23	0.22	0.22	0.20	0.20	0.19	0.19	0.21	0.20	0.22
MgO	9.93	8.63	7.59	8.78	9.06	8.19	7.29	7.63	6.48	7.47	5.61
CaO	11.60	11.00	10.15	11.97	11.84	10.90	9.58	10.35	10.25	10.92	9.67
Na_2O	2.29	2.56	3.87	2.53	2.09	2.83	3.09	2.91	5.13	2.95	3.95
BaO	0.03	0.02	0.04				0.03	0.04			0.05
K_2O	0.80	0.73	1.48	0.74	0.39	0.88	1.04	1.04	1.72	1.07	1.33
P_2O_5	0.52	0.47	0.88	0.77	0.78	0.60	0.74	0.88	1.27	0.85	1.16
Cr_2O_3	0.06	0.04	0.03				0.04	0.04			0.01
SrO	0.07	0.07	0.11				0.09	0.10			0.14
LOI	−0.47	0.00	−0.39	−0.33	1.80	−0.42	−0.18	−0.31	0.16	0.75	−0.29
	99.73	**99.64**	**99.82**	**99.68**	**100.55**	**99.56**	**99.77**	**99.84**	**100.17**	**100.27**	**99.66**
Ba	180	190	320	296	242	219	250	270	425	304	330
Cr	229	160	125	223	284	161	111	151	95	190	34
Cu	34.2	51.3	34.2	99	61.3	30	61.8	38.9	46	78	35.2
Ga	22.7	22.4	23.5	24	23.5	23	24.5	25.7	25	25.2	24.9
La	35.4	30.5	68.7	42.3	40	30.8	47.1	53.2	86.6	47.7	60.2
Nb	45.2	39.3	71	49	46.4	42	57.1	62.6	99	57.4	69.5
Ni	131.5	127.5	84.7	138	160	75	118.5	98.8	93	119	35.9
Pb	1.5	2.5	3.1	1.1	0.73	0.5	2.4	2.6	6	2.17	3.1
Rb	18	12.8	39.3	15	6.64	18	23	25.3	47	26.2	29.8
Sc	29.3	24.6	16.6	27.7	28.3	23.7	20.2	21.1	13.1	23.6	14
Sr	550	600	955	783	768	712	789	854	1238	943	1200
Th	3.8	3.6	6.8	3.46	3.57	2.5	5.3	5.9	9.25	4.44	6.3
U	1	1	1.6	0.95	0.96	0.64	1.5	1.5	2.9	1.15	1.8
V	350	332	189	330	416	287	249	312	173	384	188
Y	27.5	24.6	37.7	34	31.5	31	31.3	32.9	35	35.7	36.5
Zn	132	126	138	143	160	127	140	146	184	165	140
Zr	232	206	398	273	264	236	294	292	419	324	342
Dy	5.44	4.71	7.09		6.16		6.04	6.51		6.86	7.1
Er	2.48	2.24	3.43		2.51		2.87	2.92		2.83	3.32
Eu	2.66	2.28	3.62	3.17	3.01	2.86	3.06	3.44	4.64	3.37	3.81
Gd	7.49	6.27	10.05		8.31		8.54	9.54		9.18	10.45
Ho	0.98	0.88	1.31		1.05		1.09	1.15		1.17	1.28
Lu	0.24	0.23	0.35	0.25	0.25	0.22	0.29	0.27	0.25	0.29	0.33
Nd	35.9	29.4	57.4	42	45.6	37.2	44.1	48.8	72	52.5	56.9
Pr	8.61	7.12	14.8		11.2		10.95	12.15		13.1	14.1
Sm	7.9	6.55	11.1	10.03	9.44	8.88	9.1	10.25	15.6	10.7	11.4
Tb	1.11	0.97	1.45	1.28	1.2	1.16	1.24	1.38	1.62	1.35	1.49
Tm	0.3	0.27	0.41		0.32		0.34	0.33		0.36	0.39
Yb	1.66	1.53	2.4	2.15	1.88	1.84	1.98	1.88	2.25	2.13	2.25
Mg#	53	51	50	50	49	49	48	47	46	46	43
Nepheline	6.29	4.82	11.04	7.27	6.5	6.01	3.2	6.08	18.75	9.59	8.05
Diopside	30.34	25.76	24.53	27.75	25.99	24.71	17.68	21.91	27.49	24.64	17.85
Olivine	20.89	19.42	17.26	19.44	23.01	18.63	19.07	18.85	13.68	19.84	15.22

Table 1C New and published whole-rock geochemical data for the Antipodes Volcano, sorted by Mg#.

	A2	110212-1	110125-9	A109	110125-6	110203-3	110203-4A	110204-1	110204-4	110203-8	A8B
	Timm et al.	Scott et al.	Scott et al.	Timm et al..	Scott et al.	Scott et al.	Scott et al.	Scott et al.	Scott et al.	Scott et al.	Timm et al.
Lat.,		49°38.387	49°41.199		49°40.968′	49°41.878′	49°41.942′	49°42.431′	49°42.598′	49°41.746′	
Long		178°48.872	178°43.991		178°48.577	178°44.454′	178°44.300′	178°45.225′	178°45.036′	178°44.823′	
SiO_2	45.13	44.90	44.50	45.22	45.50	45.90	48.30	52.40	53.90	53.50	53.16
TiO_2	2.89	2.96	3.99	3.75	3.46	3.78	2.57	1.56	1.40	1.32	1.14
Al_2O_3	14.77	14.60	15.45	15.82	16.05	16.05	16.30	17.05	17.40	17.20	17.43
Fe_2O_3	1.39	13.85	14.55	1.49	13.50	13.95	13.25	11.90	10.60	11.10	1.12
FeO	12.40			13.29							9.93
MnO	0.20	0.21	0.19	0.19	0.19	0.20	0.21	0.24	0.22	0.25	0.24
MgO	4.99	4.92	5.09	4.89	4.46	4.59	3.43	1.94	1.64	1.65	1.48
CaO	8.98	9.10	9.54	9.04	9.19	8.98	7.70	5.46	5.03	4.97	4.59
Na_2O	5.82	6.11	4.15	4.28	4.60	4.41	5.05	6.48	6.35	6.70	5.70
BaO		0.07	0.04		0.05	0.04	0.06	0.07	0.07	0.08	
K_2O	2.04	2.08	1.39	1.46	1.54	1.48	1.86	2.52	2.72	2.71	2.78
P_2O_5	1.24	1.32	1.06	0.95	1.28	0.91	1.16	0.76	0.65	0.59	0.46
Cr_2O_3		0.01	0.01		0.01	0.01	0.01	<0.01	<0.01	<0.01	
SrO		0.15	0.12		0.13	0.11	0.12	0.11	0.10	0.10	
LOI	0.24	−0.56	−0.23	0.39	−0.08	−0.59	−0.15	−0.66	−0.19	−0.35	1.20
	100.09	**99.72**	**99.85**	**100.77**	**99.88**	**99.82**	**99.87**	**99.83**	**99.89**	**99.82**	**99.23**
Ba	554	520	320	347	400	370	470	590	580	630	670
Cr	48.3	36	14	18.9	5	4	6	1	2	1	1.9
Cu	35.3	37.8	33.5	16.8	23	16.2	23.7	9.9	11	11.6	11.4
Ga	29.4	28.8	25.5	26.7	28.1	27.9	26.7	29	28.4	29.8	30.9
La	94.2	98.6	51.4	48.6	75.7	51.4	70.8	84.6	62.5	88.2	92.5
Nb	95.7	113	66	65	76.8	75.2	91.3	114	116	124.5	124
Ni	52.6	52.2	23.5	13.3	16.3	12.3	11.2	6.8	5.3	4.7	1.2
Pb	4.71	6.1	2.4	2.22	2.7	2.8	3.5	4.7	5.1	5.1	5.07
Rb	53.7	46.9	25.6	31.6	36	19	35.7	60.4	39.2	63.5	62.9
Sc	9.71	8.5	15.1	12.7	12.1	12.6	9.2	4.7	3.4	4.5	3.44
Sr	1382	1385	1090	1009	1205	1070	1085	948	833	905	871
Th	11.1	11.9	5	4.54	8.6	5.4	7.5	10.8	8.9	11.5	10.6
U	3.12	3.5	1.4	1.27	2.3	1.7	2.1	2.9	2.5	3.1	3.06
V	160	140	174	184	138	174	59	4	3	1	2.12
Y	39.1	36.2	36.5	39.8	40.5	34.9	41.9	39.3	34.4	42.3	49.1
Zn	201	187	142	161	157	155	159	179	176	181	190
Zr	501	477	294	354	388	355	430	579	577	634	643
Dy	7.99	7.55	7.39	7.64	8.17	7.11	8.1	7.49	6.68	7.88	9
Er	2.97	3.19	3.22	3.14	3.64	3.3	3.86	3.77	3.49	4.05	4.14
Eu	4.58	4.64	3.95	3.78	4.45	3.65	4.39	4.09	3.4	4.12	3.91
Gd	12.2	12.5	10.85	10.3	12.3	10.15	12	10.9	8.93	11.05	11.3
Ho	1.28	1.27	1.29	1.31	1.43	1.28	1.46	1.39	1.26	1.48	1.6
Lu	0.27	0.28	0.3	0.31	0.34	0.31	0.4	0.42	0.41	0.47	0.49
Nd	84	78.3	54.4	56.4	67.3	50.9	67	67	53.5	68.1	77.8
Pr	22.6	20.4	13.05	13.8	16.95	12.4	16.7	17.85	14.15	18.4	21.7
Sm	15.3	14.4	11.8	11.7	13.5	10.75	13.2	12.2	9.99	12.35	13.8
Tb	1.7	1.7	1.55	1.5	1.73	1.46	1.71	1.56	1.33	1.62	1.72
Tm	0.36	0.36	0.37	0.4	0.42	0.39	0.47	0.47	0.44	0.51	0.57
Yb	2.1	1.99	2.09	2.36	2.38	2.2	2.7	2.83	2.67	3.06	3.53
Mg#	42	41	41	40	40	39	34	24	23	23	21
Nepheline	19.85	21.79	8.65	8.78	9.16	7.91	6.91	9.5	6.59	9.48	3.78
Diopside	23.66	25.55	17.7	15.9	15.69	16.02	12.2	10.52	8.45	10.38	5.19
Olivine	12.97	10.95	13.62	15.75	12.73	12.94	13	10.72	9.75	9.7	12.61

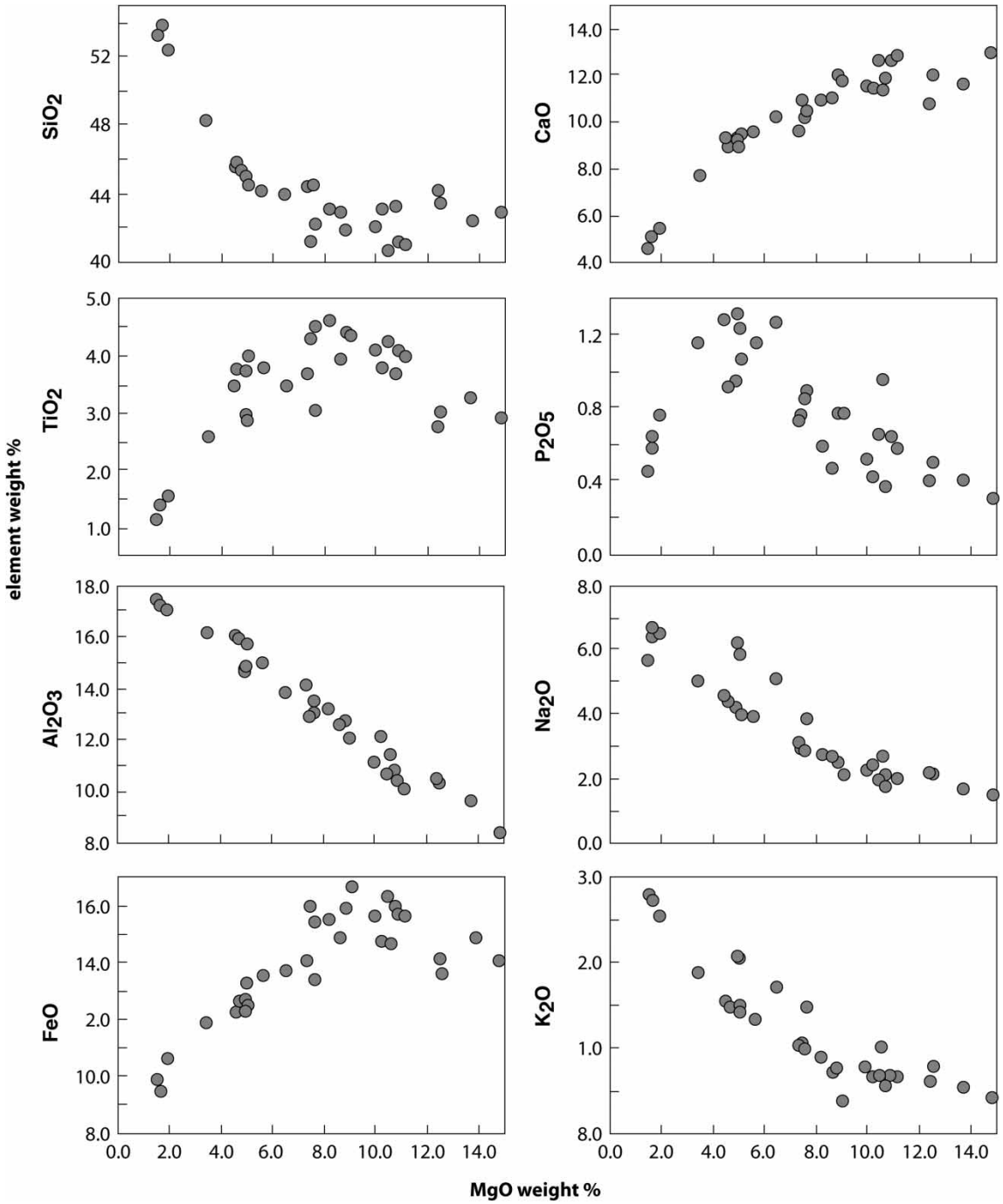

Figure 7 Fenner diagrams for selected major elements illustrate the trend in major elements in the sample suite. Iron is reported as total FeO.

decrease at c. 8 wt% MgO. Similarly, P_2O_5 and Sr contents begin to drop at 4–6 wt% MgO (Figs 7, 8). The highest Cr and Ni contents correspond to lavas with highest MgO, whereas Ba, Ce, Y and Zr have the inverse relationship (Fig. 8). Primitive-mantle normalised data reveal that rocks with low Mg# have higher elemental contents than high Mg# rocks (Fig. 9A) and also that all data are similar to the average composition of Ocean Island Basalt of Sun & McDonough (1989). Samples Ant-7 (Panter et al. 2006), A2 (Timm et al. 2010) and 110212-1 (this study) from lavas on Reef Point on the northeast corner of the island (Fig. 6A) all have anomalous Pb for their given MgO contents (Table 1A–C).

A distinctive geochemical characteristic is that every sample in the Antipodes Volcano dataset shows a depletion of K and Pb normalised to primitive mantle (Fig. 9A). Compared to the well-studied alkaline intraplate Dunedin Volcanic Group on the New Zealand mainland of broadly the same SiO_2 range, the Antipodes Volcano basanites are

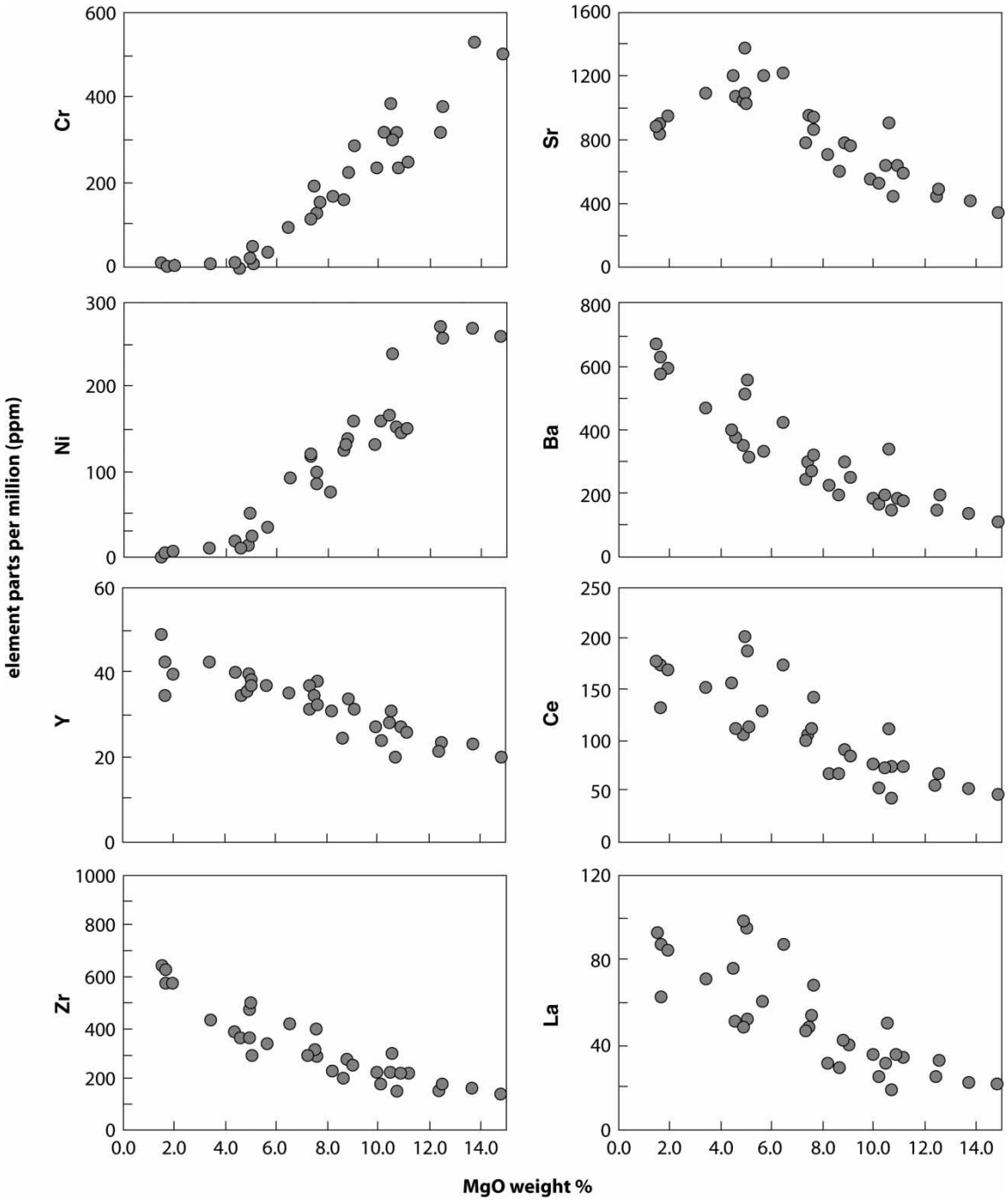

Figure 8 Fenner diagrams for selected minor elements illustrate the trend in major elements in the sample suite.

similar except that they generally have more extreme negative K and Pb anomalies (Fig. 9A). Other large-ion lithophile elements such as Rb, Ba and Sr at equivalent SiO_2 extend to slightly lower normalised contents in the Antipodes Volcano relative to the Dunedin Volcanic Group. Chondrite-normalised rare Earth element (REE) plots for the Antipodes Volcano demonstrate significantly higher light rare Earth elements (LREEs) relative to heavy rare Earth element (HREE) contents ($(La/Lu)_N = 13–28$). A plot of chondrite-normalised La/Sm shows that LREE increase slightly with decreasing MgO (Fig. 9B), but the overall high LREE/HREE ratio remains prevalent.

Discussion

Petrological evolution of the Antipodes Volcano

The paucity of graded or cross bedding in pyroclastic rocks, the absence of pillow lavas and the baked peat beneath a lava flow

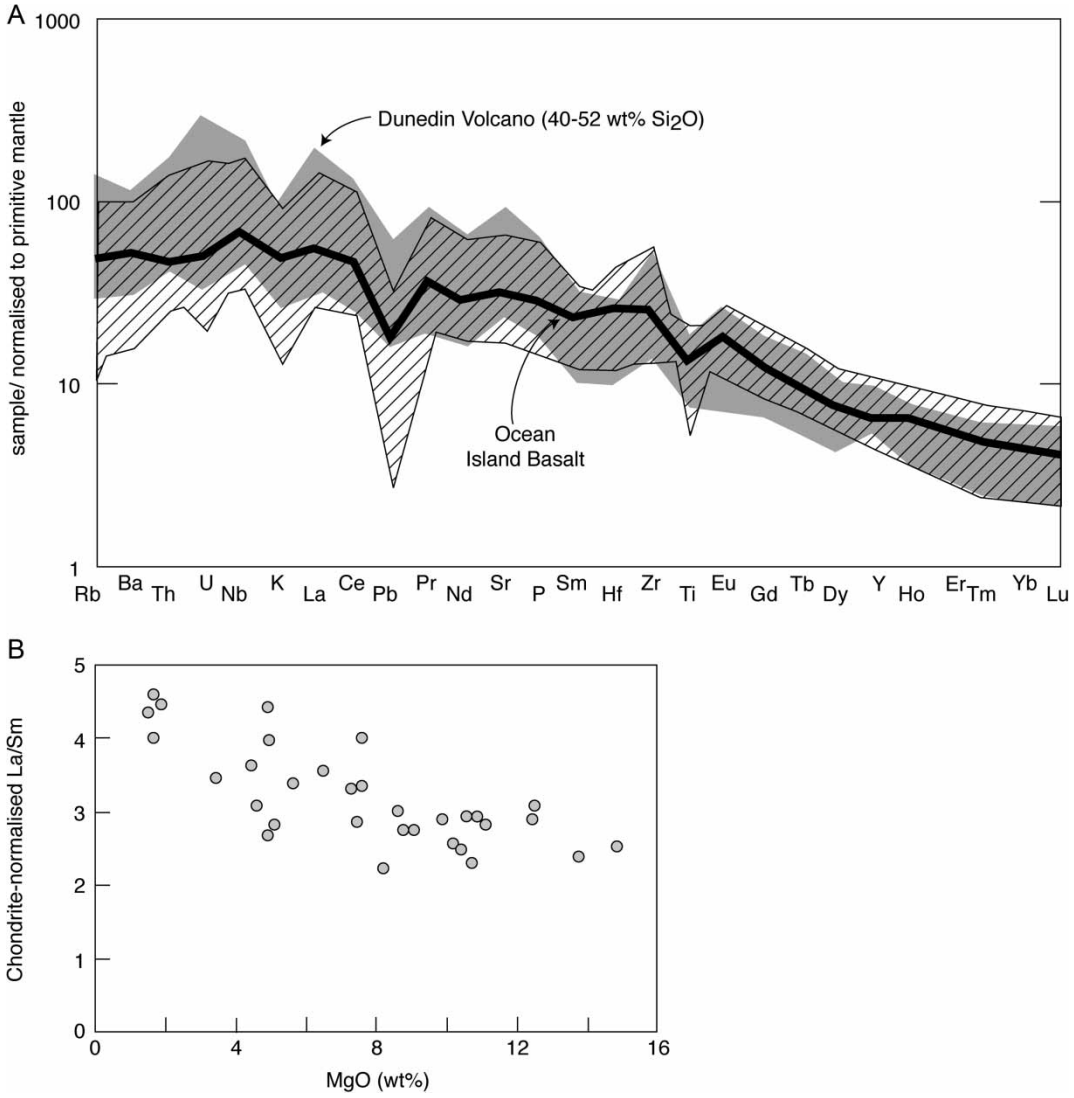

Figure 9 A, Trace-element data normalised to primitive mantle (Sun & McDonough 1989), with the Dunedin Volcano (hatched; from Coombs et al. 2008) and Ocean Island Basalt plotted for comparison. See the Data Supplementary file for complete primitive mantle-normalised and chondrite-normalised plots. **B**, Chondrite-normalised La/Sm versus MgO, illustrating the increase in LREE content with fractionation.

imply that most of the exposed rocks on the Antipodes Islands were deposited sub-aerially. The intercalation of pyroclastic rocks and lavas points to there having been multiple Pleistocene eruptive events; the published Ar/Ar ages (Timm et al. 2010) and also the pollen and spores in peat beneath the lava on the eastern side of the island indicate that these events were closely spaced in time and occurred in the last 500 ka. The picture of the complete volcano is one of numerous, spatially overlapping and temporally closely spaced, emergent tuff cones that regularly emitted basaltic lavas. The variable geographic continuity of lavas probably represents the flows having been controlled by palaeotopography caused by the tuff cone arrangement. Small cinder cones are especially prominent on the northeast of the main island. As the chemistry of these cinder cones is not distinguishable from lava elsewhere on the island, these probably represent the last phase of terrestrial magmatism associated with the Antipodes Volcano.

No vertical chemical stratigraphy in the crystalline rocks could be established, but there are broad geographical differences. The most primitive rocks (picrobasalt; Mg# = 65–62) occur on the north-eastern corner of the main island, whereas more evolved trachyandesite and tephra-phonolite (Mg# = 23–24) occur on the south-western corner (Fig. 6C). In detail, however, the distribution of rock types is more complex because the most evolved lava is feldspar-bearing A8b (Mg# = 21) that occurs on the eastern side of the island, whereas a porphyritic dyke with a relatively primitive composition (110201-4; Mg# = 56) occurs on the south-western side. The lava compositions probably represent repeated tapping of a magma chamber.

The presence of extremely rare granite clasts in pyroclastic debris suggests that the Antipodes Volcano magma interacted with the continental crust. However, highly incompatible element ratios sensitive to continental crustal input, such as Ba/Nb (Fig. 10A) or Ce/Pb (Fig. 10B) versus MgO, point to little variation across the entire suite of samples. A Nb/Th versus Nb/U plot indicates that the data plot between primitive mantle and a depleted mantle end-member (Fig. 10C) and that there was either less than 1% crustal contamination or there was no crustal contamination, and the spread in ratios represents two mantle source regions. Either way, the small granite clasts probably represent fortuitously plucked material from shallow

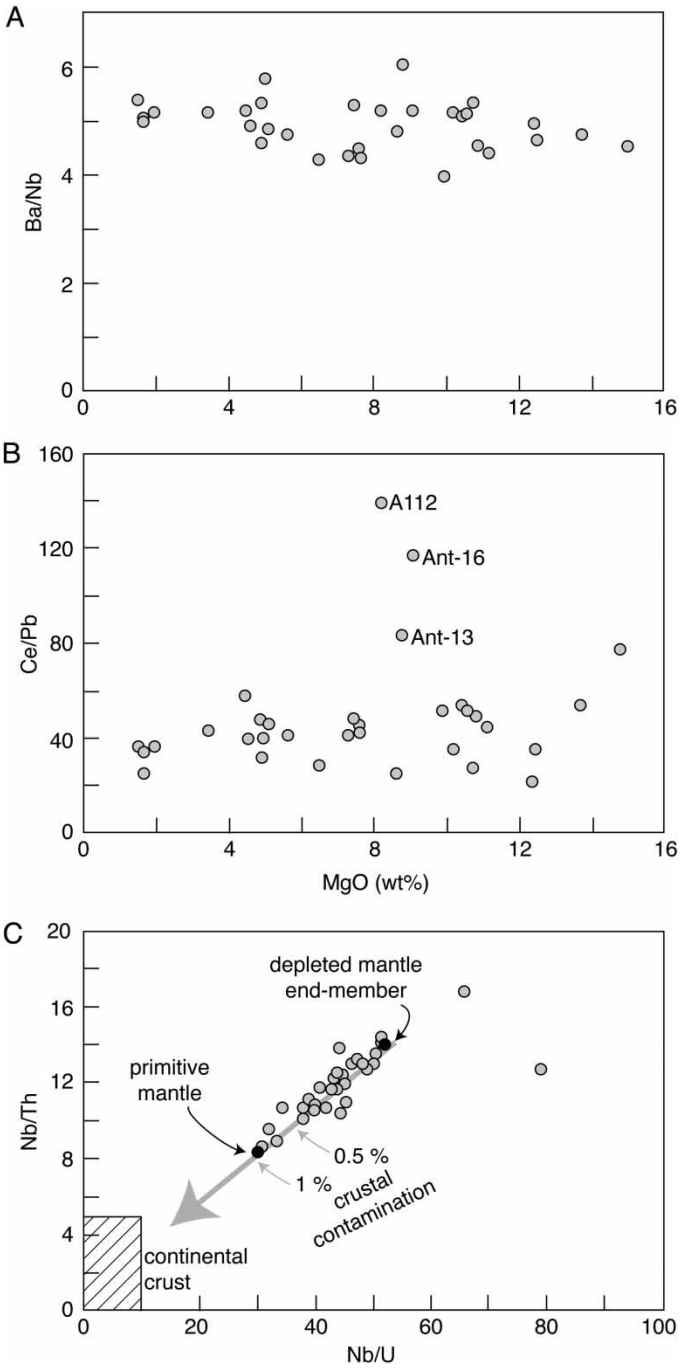

Figure 10 **A**, Ba/Nb versus MgO plot illustrating the lack of variation in very incompatible elements versus fractionation. **B**, Ce/Pb versus MgO plot illustrating the general lack of variation in moderately incompatible elements versus fractionation. The three samples with distinctly high Ce/Pb ratios have anomalously low Pb contents for their MgO and come from the interior of the island. **C**, Nb/Th versus Nb/U plot. The majority of data plot on a tight array indicating minimal (<1%) crustal contamination, consistent with the results of the Ba/Nb and Ce/Pb plots. Modified from Sylvester et al. (1997).

Table 2 Summary of published age-corrected Sr–Nd–Pb isotopic data sorted by whole-rock Mg# for Antipodes Volcano lavas.

Sample No.	Mg#	$^{87}Sr/^{86}Sr$ (initial)	$^{143}Nd/^{144}Nd$ (initial)	$^{206}Pb/^{204}Pb$ (initial)	$^{207}Pb/^{204}Pb$ (initial)	$^{208}Pb/^{204}Pb$ (initial)	Data source
Ant 3	53	0.702930 ± 20	0.512921 ± 10	20.608	15.693	39.906	Panter et al. (2006)
		(0.702929)	(0.512920)	(20.604)	(15.693)	(39.894)	
A105	53	(0.702939)	(0.512914)	(20.507)	(15.656)	(39.759)	Timm et al. (2010)
Ant 13	50	0.702934 ± 17	0.512913 ± 11	20.532	15.657	39.739	Panter et al. (2006)
		(0.702934)	(0.512913)	(20.528)	(15.657)	(39.723)	
Ant 16	49	0.702903 ± 15	0.512911 ± 10	20.492	15.651	39.728	Panter et al. (2006)
		(0.702902)	(0.512911)	(20.485)	(15.651)	(39.700)	
A109	40	(0.702904)	(0.512917)	(20.493)	(15.652)	(39.730)	Timm et al. (2010)

crustal levels. These interpretations are supported by published radiogenic $^{143}Nd/^{144}Nd$ values (0.51291–0.51292) and unradiogenic $^{87}Sr/^{86}Sr$ values (0.70290–0.70294) of several Antipodes Volcano lavas (Table 2; Panter et al. 2006; Timm et al. 2010), which also indicate little or no crustal contamination.

The large geochemical dataset for a temporally related lava suite means that constraints can be placed upon interpretations of how and where crystal fractionation took place. The lack of variation in MgO versus incompatible element ratios Ba/Nb (Fig. 10A), Ce/Pb (Fig. 10B) and Nb/Zr (not shown) indicates a shared liquid line of descent for the entire lava suite. The calculated chondrite-normalised La/Lu variation (13–28) and the increase in LREE with decreasing MgO (Fig. 9B) probably reflect crystal fractionation dominated by pyroxene and olivine. Similarly, the small scatter in K_2O or TiO_2 at given MgO (Fig. 7) may also be a result of fractionation. An FeO versus MgO plot indicates that the least fractionated crystalline rocks (110122-11, 110128-18, A6, 110201-4) were in equilibrium with peridotite olivine of Fo_{87-88} composition (Fig. 11A). Because these rocks also have the highest Cr contents (Table 1A–C), they cannot have accumulated significant olivine and are therefore the closest to the parental composition. The remainder of the crystalline rock dataset plots as if in equilibrium with less Mg-rich olivine and shows decreasing CaO with MgO (Fig. 7), indicative of olivine and clinopyroxene fractionation. The proportion of normative olivine, clinopyroxene and nepheline components forms an array between the 1 bar and limiting 8–30 kbar cotectics of Sack et al. (1987), which is also consistent with fractionation of olivine and clinopyroxene at relatively low $P < 8$ kbar (Fig. 11B). This moderate- to low-pressure estimate leads to the conclusion that crystal fractionation most likely occurred within a magma chamber(s) within continental crust – although evidently undergoing little crust–magma interaction in the investigated rocks – and that this chamber was repeatedly tapped to produce Surtseyan-like eruptions and lava flows that coalesced to form the Antipodes Islands.

Mantle source region

With the array of geochemical and isotopic data available, it is possible to provide a comprehensive analysis of the mantle

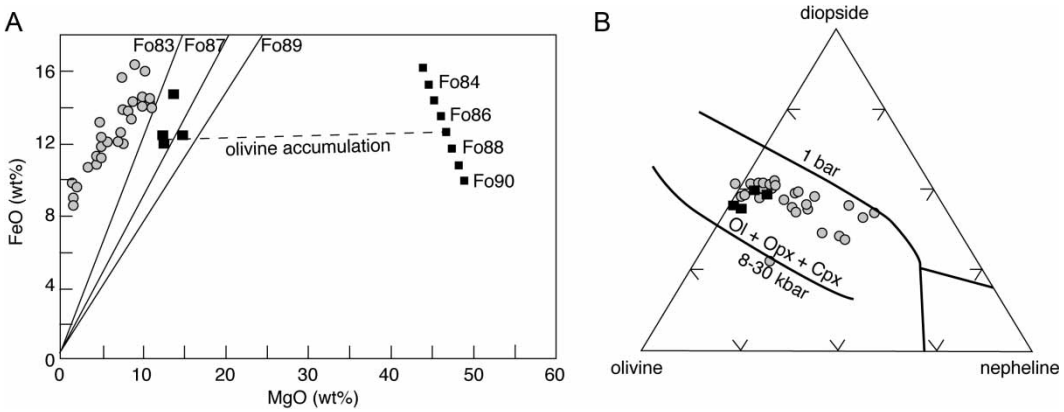

Figure 11 A, FeO–MgO diagram for Antipodes lavas (data of this study only), illustrating a lack of olivine accumulation in the suite. The most primitive magmas are the four black boxes on the left-hand side. **B**, Proportions of normative diopside, olivine and nepheline components in Antipodes Volcano lavas compared to 1 bar and limiting 8–30 kbar cotectics according to Sack et al. (1987). The four most primitive magmas are the shown as black boxes. The array of data between the cotectics indicates fractionation of olivine ± clinopyroxene at relatively low pressures.

source to the Antipodes Volcano. The geochemical data show all the crystalline rocks to be LREE-enriched and HREE-depleted relative to primitive mantle (Fig. 9) or chondrite (data supplementary). Because the variation in LREE/HREE values is inferred to be due to crystal fractionation and the overall elevated LREE/HREE signature ubiquitous (see above), these distinctive compositions must be due to either low-degree partial melting and/or a LREE-enriched source region imparted an imprint on the REE budget of the derived melts. The low HREE contents in the least fractionated samples are consistent with residual garnet in the source region (e.g. Kay & Gast 1973). Elevated CaO at high MgO (Fig. 7) is interpreted to show that the source was more likely to have been peridotite than pyroxenite (e.g. Herzberg & Asimow 2008).

Given the apparently primitive composition and lack of continental crust interaction, the Sr, Nd and Pb isotopes from the Antipodes Volcano lavas (Table 2) should closely reflect the isotopic composition of the peridotitic mantle source region. The highly radiogenic $^{206}Pb/^{204}Pb$ ratios (20.5–20.6) and unradiogenic $^{87}Sr/^{86}Sr$ (0.70290–0.70294) are indicative of a HIMU-like mantle component (e.g. Stracke et al. 2005; Panter et al. 2006; Timm et al. 2010). A variably diluted HIMU-like isotopic character has been inferred as a source component to many of the intraplate volcanoes across New Zealand (Fig. 12), although the revision in nomenclature by Stracke et al. (2005) means that several New Zealand cases could also be classified as having a FOZO (focal zone) reservoir (Fig. 12A, B). However, the Antipodes Volcano has some of the consistently highest $^{206}Pb/^{204}Pb$ and $^{143}Nd/^{144}Nd$ and lowest $^{87}Sr/^{86}Sr$ ratios across the intraplate suite (a selection of data are shown on Fig. 12A, B; see Timm et al. 2010 for a comprehensive presentation) and, unlike the other offshore sub-aerial Zealandia intraplate volcanoes (Chatham Islands, Auckland Islands or Campbell Island), the Antipodes Volcano data is consistent with a wholly HIMU-like mantle reservoir. The clarity of the Antipodes Volcano HIMU-like signature may represent minimal interaction between magma and the overlying lithosphere during ascent. This interpretation is supported by the occurrence of HIMU-like isotopic compositions in some 25 Ma peridotite xenoliths from Zealandia intraplate volcanoes (Fig. 12; Waight et al. 2013), which represent fragments of the upper Zealandia mantle at the time of volcanism.

The ubiquitous negative Pb and K anomalies present in all Antipodes Volcano lavas (Fig. 9) occur in intraplate mafic volcanic rocks throughout the DAMP (e.g. Baker et al. 1994; Finn et al. 2005; Panter et al. 2000, 2006; Hoernle et al. 2006, 2010; Sprung et al. 2007; Timm et al. 2010). Such trace-element signatures have been attributed to the retention of Pb and K in residual amphibole $\pm$ phlogopite $\pm$ sulphide during melting of a modally metasomatised lithospheric source (Class & Goldstein 1997; Panter et al. 2006). Alternatively, the negative anomalies may reflect a source region from which the incompatible Pb and K (and other elements that cannot readily be discerned from the geochemical data) had been preferentially removed at some earlier stage. This latter interpretation is partially supported by the occurrence of negative K and Pb anomalies in the anhydrous Zealandia peridotite xenolith suite (Waight et al. 2013; Scott et al. unpubl. data). As amphibole and/or biotite are typically absent in the peridotites, the K anomalies probably represent previous extraction of this fluid mobile element. If the intraplate basalts do have a lithospheric mantle source (or a contribution), then the extreme negative K and Pb anomalies could be due to inheritance of mantle trace-element signatures rather than requiring melting of a veined mantle that had residual amphibole, mica or sulphide (cf. Panter et al. 2000, 2006; Sprung et al. 2007).

Weaker HIMU-like compositions in some of the other Zealandia intraplate volcanoes have been attributed to mixing of HIMU-like and enriched mantle components (Hoernle et al. 2006) or continental crust (Panter et al. 2006). However, an important observation is that the spread in Pb isotopes within the peridotite suite demonstrates that the Zealandia lithospheric mantle is far from isotopically uniform (Fig. 12A, B). There appear to be domains in which the HIMU-like signature is strong and others where it is weak or non-existent. The Antipodes Volcano source evidently melted a HIMU-like mantle domain but some of other intraplate volcanoes may have sampled less-radiogenic Pb domains. The Antipodes Volcano therefore preserves compelling evidence for an end-member HIMU-like mantle reservoir within the Zealandia lithosphere, making the geochemical and isotopic dataset an excellent baseline for HIMU-like intraplate volcanism within the southwest Pacific DAMP.

Conclusions

The Antipodes Volcano is a strongly alkaline Pleistocene suite of lavas and tuff cones that rises above sea level at the very edge of the Campbell Plateau. The <0.5 Ma volcano appears to be extinct, and has been dissected by the Pacific Ocean. The excellent coastal exposure indicates that the volcano likely formed by repeated tuffaceous Surtseyan-like eruptions that were accompanied by small extrusions of lava. Magma differentiation was achieved by fractionation of olivine and clinopyroxene at relatively low pressure within the continental crust beneath the volcanic centre. Geochemical parameters and published isotopic compositions indicate that the ascending magmas underwent little or no interaction with the continental crust; the Antipodes Volcano therefore contains one of the clearest signals of an end-member HIMU-like mantle source region for the Zealandia intraplate basalts. The Zealandia lithospheric mantle is not isotopically homogeneous, especially in terms of Pb, and weaker HIMU signatures in other intraplate volcanoes may not necessarily require HIMU-like mantle source component.

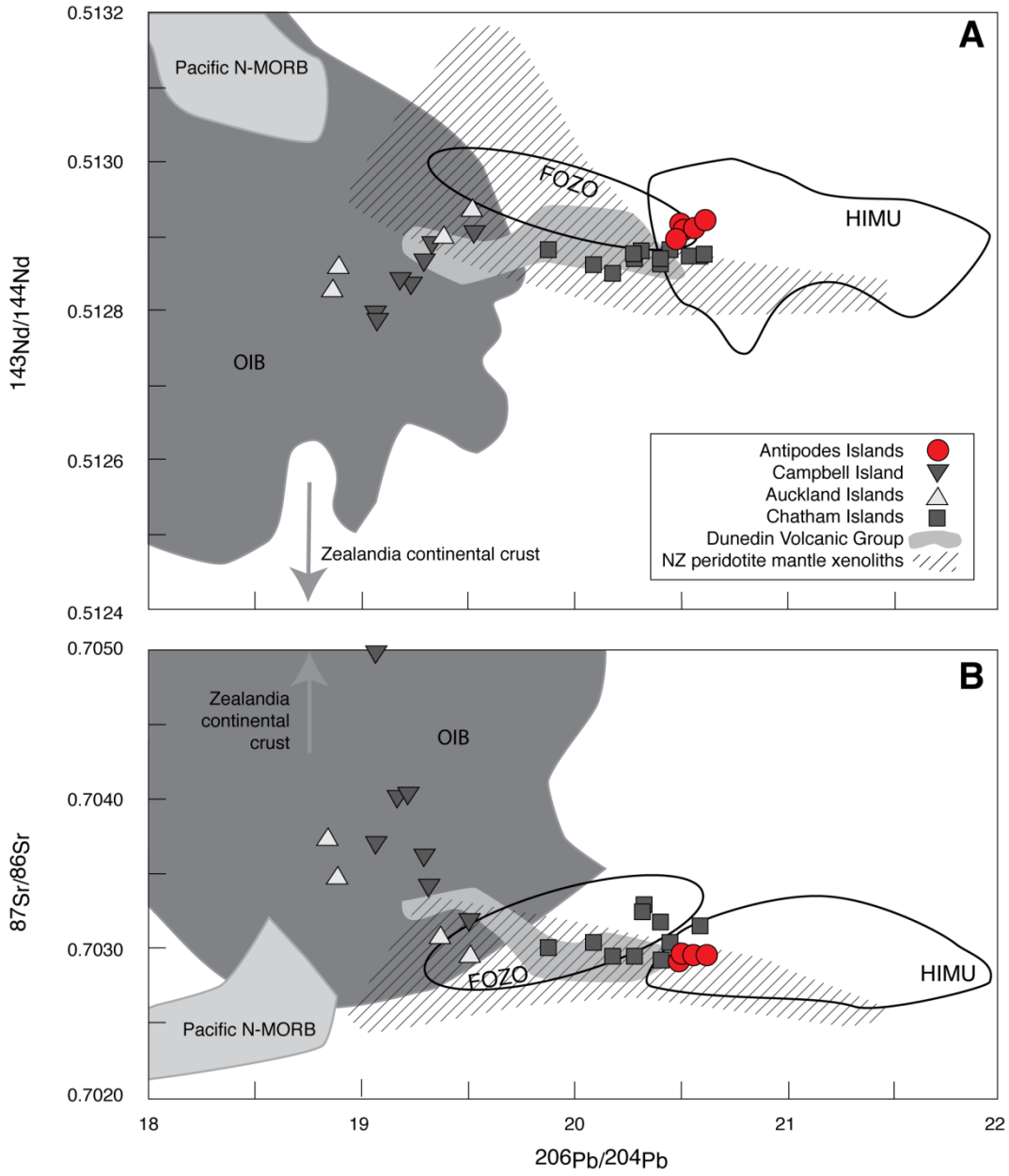

Figure 12 A, Nd–Pb and **B**, Sr–Pb isotope plots showing the Antipodes Volcano compared with isotope data from basalts from the Dunedin Volcanic Group (c. 16–11 Ma), Auckland Islands (16 Ma), Campbell Island (16–7 Ma), Chatham Islands (85 and 5 Ma) and Zealandia peridotite xenoliths (c. 34–10 Ma). Radiogenic ingrowth for the Dunedin Volcanic Group, Auckland Islands, Campbell Island, Pliocene Chatham Islands and the peridotite xenolith data is insignificant relative to the scale of the diagram, and the measured isotopic ratios are plotted. The Cretaceous Chatham Islands data is plotted with model source compositions. Data from Hoernle et al. (2006), Panter et al. (2006), Timm et al. (2010) and Waight et al. (2013). Mantle classification fields are positioned for present-day isotopic compositions (Stracke et al. 2005).

Supplementary file

Figure S1. Trace-element-normalised concentrations for individual whole-rock analyses.
Top: Individual lava trace elements normalised to the composition of primitive mantle. Bottom: Individual lava rare Earth elements normalised to the composition of chondrite. Normalising values are from Sun & McDonough (1989).

Acknowledgements

We thank Pete McCelland for permission to land and collect rocks; Paul Sagar for the opportunity to go to the Antipodes Islands; Henk Haazen and the RV *Tiama* for transport to and from the islands; James White, Quinten van der Meer and Tod Waight for comments on the manuscript; Christian Timm and Karsten Haase for journal reviews; and Matthew Leybourne for editorial handling. Funding was provided by a Foundation

for Research Science and Technology contract UOOX1004 to JMS.

References

Adams CJ 1985. Geology of the Antipodes and Bounty Islands, Southwest Pacific. Report of geological studies on the 1985 Subantarctic cruise of HMNZS Monowai: northern leg to Antipodes and Bounty Islands, 27 February–13 March 1985. Institute of Nuclear Sciences Report INS-R-300. Institute of Nuclear Sciences, DSIR, Lower Hutt, New Zealand.

Baker JA, Gamble JA, Graham IJ 1994. The age, geology and geochemistry of the Tapuaenuku Igneous Complex, Marlborough, New Zealand. New Zealand Journal of Geology and Geophysics 37: 24–268.

Barreiro BA, Cooper AF 1987. A Sr, Nd and Pb isotope study of alkaline lamprophyres and related rocks from Westland and Otago, South Island, New Zealand. Geological Society of America Special Paper 215: 115–125.

Class C, Goldstein SL 1997. Plume–lithosphere interactions in the ocean basins; constraints from the source mineralogy. Earth and Planetary Science Letters 150: 245–260.

Coombs DS, Cas RA, Kawachi Y, Landis CA, McDonough WF, Reay A 1986. Cenozoic volcanism in North, East, and Central Otago. In: Smith IEM ed Late Cenozoic volcanism in New Zealand. Royal Society of New Zealand Bulletin 23: 278–312.

Coombs DS, Adams CJ, Roser BP, Reay A 2008. Geochronology and geochemistry of the Dunedin Volcanic Group, eastern Otago, New Zealand. New Zealand Journal of Geology and Geophysics 51: 195–218.

Cullen DJ 1969. Quaternary volcanism at the Antipodes Islands, It's bearing on structural interpretation of the Southwest Pacific. Journal of Geophysical Research 74: 4213–4220.

Finn CA, Müller RD, Panter KS, 2005. A Cenozoic diffuse alkaline magmatic province (DAMP) in the southwest Pacific without rift or plume. Geochemistry, Geophysics, Geosystems 6. doi:10.1029/2004GC000723

Fleming CA, 1965. Two-storied cliffs at the Auckland Islands. Transactions of the Royal Society of New Zealand, Geology 3: 171–174.

Gamble JA, Adams CJ 1990. Antipodes Islands. In: LeMasurier WE, Thompson JW eds. Volcanoes of the Antarctic Plate and Southern Oceans. American Geophysical Union, Antarctic Research Series 48: 468–469.

Gamble JA, Morris PA, Adams CJ 1986. The geology, petrology and geochemistry of Cenozoic volcanic rocks from the Campbell Plateau and Chatham Rise. In: Smith IEM ed. Late Cenozoic volcanism in New Zealand. Royal Society of New Zealand Bulletin 23: 344–365.

Gill R 2010. Igneous rocks and processes: a practical guide. Oxford: Wiley-Blackwell.

Hector J 1870. Notes on the geology of the outlying islands of New Zealand with extracts from official reports. Transactions of the New Zealand Institute 2: 176–186.

Herzberg C, Asimow PD 2008. Petrology of some oceanic islands basalts: PRIMELT2.XLS software for primary magma calculation. Geochemistry, Geophysics, Geosystems 9. doi:10.1029/2008GC002057

Hoernle K, White JDL, van den Bogaard P, Hauff F, Coombs DS, Werner R, Timm C, Garbe-Schönberg D, Reay A, Cooper AF 2006. Cenozoic intraplate volcanism on New Zealand: upwelling induced by lithospheric removal. Earth and Planetary Science Letters, 248: 335–352.

Hoernle K, Hauff F, van den Bogaard P, Werner R, Mortimer N, Geldmacher J, Garbe-Schönberg D, Davy B 2010. Age and geochemistry of volcanic rocks from the Hikurangi and Manihiki oceanic Plateaus. Geochemica et Cosmochimica Acta 74: 7196–7219.

Kay RW, Gast PW 1973. The rare earth content and origin of alkali-rich basalts. The Journal of Geology 81: 653–682.

Lanyon R, Varne R, Crawford AJ 1993. Tasmanian Tertiary basalts, the Balleny plume, and opening of the Tasman Sea (southwest Pacific Ocean). Geology 21: 555–558.

Le Maitre RW, Streckeisen A, Zanettin B, Le Bas MJ, Bonin B, Bateman P eds. 2002. Igneous Rocks: A Cassification and Glossary of Terms: Recommendations of the International Union of Geological Sciences Subcommission on the Systematics of Igneous Rocks. Cambridge University Press, Cambridge.

Lorenz V 1974. Studies of Surtsey tephra deposits. Surtsey Research Program Report 7: 72–79.

McCoy-West AJ, Baker JA, Faure K, Wysoczanski R 2010. Petrogenesis and origins of mid-Cretaceous continental intraplate volcanism in Marlborough, New Zealand: implications for the long-lived HIMU magmatic mega-province of the SW Pacific. Journal of Petrology 51: 2003–2045.

McGlone MS, Meurk CD 2000. Modern pollen rain, subantarctic Campbell Island, New Zealand. New Zealand Journal of Ecology 24: 181–194.

Morris PA 1985a. Petrology of Late Cretaceous alkaline volcanic rocks from the Chatham Islands, New Zealand. New Zealand Geology and Geophysics 28: 253–266.

Morris PA 1985b. The geochemistry of Eocene–Oligocene volcanics on the Chatham Islands, New Zealand. New Zealand Journal of Geology and Geophysics 28: 459–469.

Mortimer N, Gans PB, Hauff F, Barker DHN 2012. Paleocene MORB and OIB from the Resolution Ridge, Tasman Sea. Australian Journal of Earth Sciences: An International Geoscience Journal of the Geological Society of Australia 59: 953–964

Panter KS, Hart SR, Kyle P, Bluzstanjn J, Wilch T 2000. Geochemistry of Late Cenozoic basalts from the Crary Mountains: characterization of mantle sources in Marie Byrd Land, Antarctica. Chemical Geology 165: 215–241.

Panter KS, Blusztajn J, Hart SR, Kyle PR, Esser R, McIntosh WC 2006. The origin of HIMU in the SW Pacific: evidence from intraplate volcanism in southern New Zealand and subantarctic islands. Journal of Petrology 47: 1673–1704.

Price RC, Cooper AF, Woodhead JD, Cartwright I 2003. Phonolitic diatremes within the Dunedin Volcano, South Island, New Zealand. Journal of Petrology 44: 2053–2080.

Reay A, Forsyth PJ, Turnbull IM 1990. Geological investigations on the Antipodes Islands. Unpublished DSIR Geology and Geophysics Immediate Report QM483/710. Dunedin, GNS Science.

Sack RO, Walker D, Carmichael ISE 1987. Experimental petrology of alkalic lavas: constraints on cotectics of multiple saturation in natural basic liquids. Contributions to Mineralogy and Petrology 96: 1–23.

Sprung P, Schuth S, Munker C, Hoke L 2007. Intraplate volcanism in New Zealand: the role of fossil plume material and variable lithospheric properties. Contributions to Mineralogy and Petrology 153: 669–687.

Stracke A, Hofmann AW, Hart SR 2005. FOZO, HIMU, and the rest of the mantle zoo. Geochemistry, Geophysics, Geosystems 6. doi:10.1029/2004GC000824

Sun S-S, McDonough WF 1989. Chemical and isotopic systematics of oceanic basalts: implications for mantle composition and processes. Geological Society, London, Special Publication 42: 313–345.

Sylvester PJ, Campbell IH, Bowyer DA 1997. Niobium/uranium evidence for early formation of the continental crust. Science 275: 521–523.

Thomson BN 1990. Antipodes Islands Group – a photogeological interpretation. New Zealand Geological Survey Report G117.

Timm C, Hoernle, K, van den Bogaard P, Bindeman I, Weaver S 2009. Geochemical evolution of intraplate volcanism at Banks Peninsula, New Zealand: interaction between asthenospheric and lithospheric melts. Journal of Petrology 50: 989–1023.

Timm C, Hoernle K, Werner R, Hauff F, van den Bogaard P, White J, Mortimer N, Garbe-Schonberg D 2010. Temporal and geochemical evolution of the Cenozoic intraplate volcanism of Zealandia. Earth Science Reviews. doi:10.1016/j.earscirev.2009.10.002.

Tulloch AJ, Ireland T, Parkinson D, Turnbull IM 2003. Nature of Eastern Campbell Plateau basement: age and character of a granite xenolith from Antipodes Island (abstract). Geological Society of New Zealand annual conference, Dunedin.

Verwoerd WJ, Chevallier L 1987. Contrasting types of surtseyan tuff cones on Marion and Prince Edward islands, southwest Indian Ocean. Bulletin of Volcanology 49: 399–417.

Waight TE, Scott JM, van der Meer QHA 2013. Isotopic characterisation of the sub-continental lithospheric mantle beneath Zealandia, a rifted fragment of Gondwana. EGU General Assembly Geophysical Research abstracts, v. 15.

Warham J, Johns PM 1975. The University of Canterbury Antipodes Island expedition 1969. Journal of the Royal Society of New Zealand 5: 103–131.

Weaver SD, Smith IEM 1989. New Zealand intraplate volcanism. In: Johnson RW ed. Intraplate volcanism in eastern Australia and New Zealand. Cambridge, Cambridge University Press. Pp. 157–188.

Zhang M, O'Reilly SY, Chen D 1999. Location of Pacific and Indian mid-ocean ridge-type mantle in two time slices: evidence from Pb, Sr, and Nd isotopes for Cenozoic Australian basalts. Geology 27: 39–42.